New Journal of Chemistry

Electronic Supplementary Information

Acquiring preferred mode of aggregation through positional antagonism for saponification triggered gelation

Prem Chand and Ashish Kumar*

Department of Chemistry, Institute of Science, Banaras Hindu University,

Varanasi - 221 005 (U.P.), India

Dilution experiment:

Stock solutions for **A-B** (c, 5.0 x 10^{-5} M) have been prepared in $CHCl_3$ for UV-vis and fluorescence spectroscopy, based on dilution experiments. It is a basic optimization step for this class of gelation to determine the highest permissible concentration that can be employed for photophysical studies. Actually, proper gelation occurs using 2.0 x 10^{-2} M concentration of **A-B** (mentioned in experimental section 2.6) which was exceedingly high to carry out photophysical studies. Therefore, an intermediate concentration less than 2.0 x 10^{-2} M had to be determined which should also be suitable for measuring photophysical data without any significant change in properties of **A-B**. On dilution from ~10^{-4} to 10^{-7} M, **A-B** did not exhibit any significant decomposition or dissociation and displayed only an obvious decrease in optical and fluorescence intensity (Fig. S10, ESI). It clearly indicated that an intermediate concentration i.e. 5.0 x 10^{-5} M can be used for UV-vis and fluorescence studies.

Preparation of stock solutions for UV-vis and fluorescence study:

10^{-2} M solutions for **A** and **B** have been prepared by dissolving 0.1 equiv. (**A**, 80.6; **B**, 101.4 mg) in 10 mL of $CHCl_3$. This solution was further diluted 200 times by adding $CHCl_3$ to obtain 5.0 x 10^{-5} M solutions which were directly used for photophysical studies.

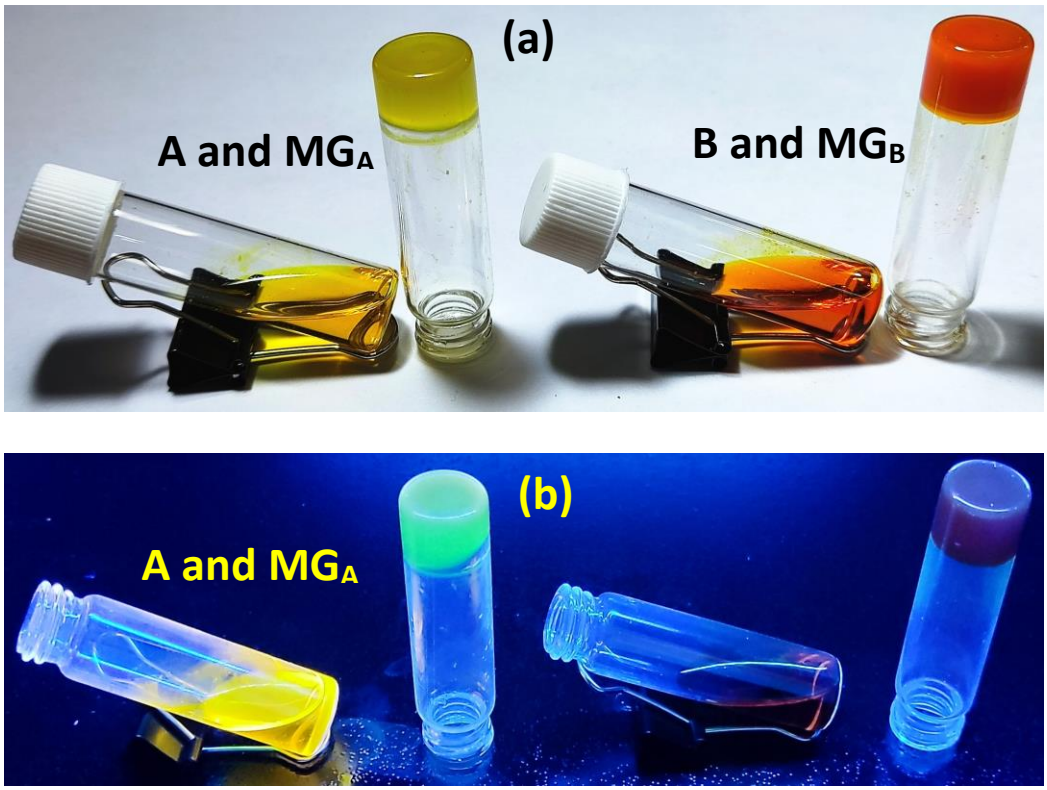

Fig. S1 (a) Demonstration of gelation using complex **A** and **B. MG_A** and **MG_B** were tested by inverted vial method. (b) **A-B** and **MG_A-MG_B** observed under UV-vis lights (λ= 365 nm).

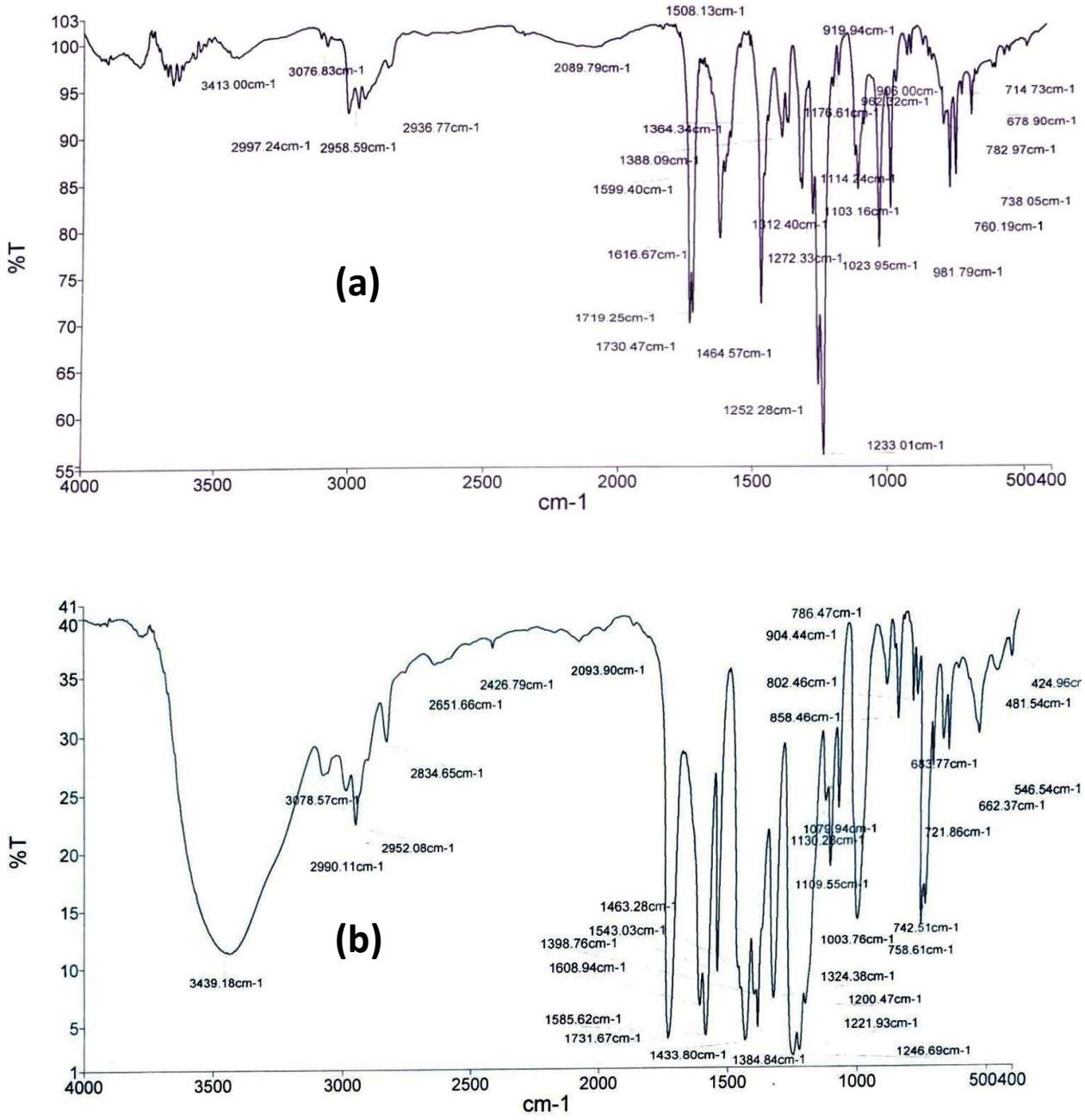

Fig. S2 FT-IR spectra for (a) **HL_A** and (b) Complex **A**. On comparing both, a significant shift in the vibration frequency associated with imine linkage from 1616 to 1608 cm^{-1} has been noted while there was no significant change in frequency of band associated with ester linked >C=O. This indicated that imine linked N has involved in coordination bonding with metal (Zn^{II}) thereby substantiating the formation of complex **A** from **HL_A**.

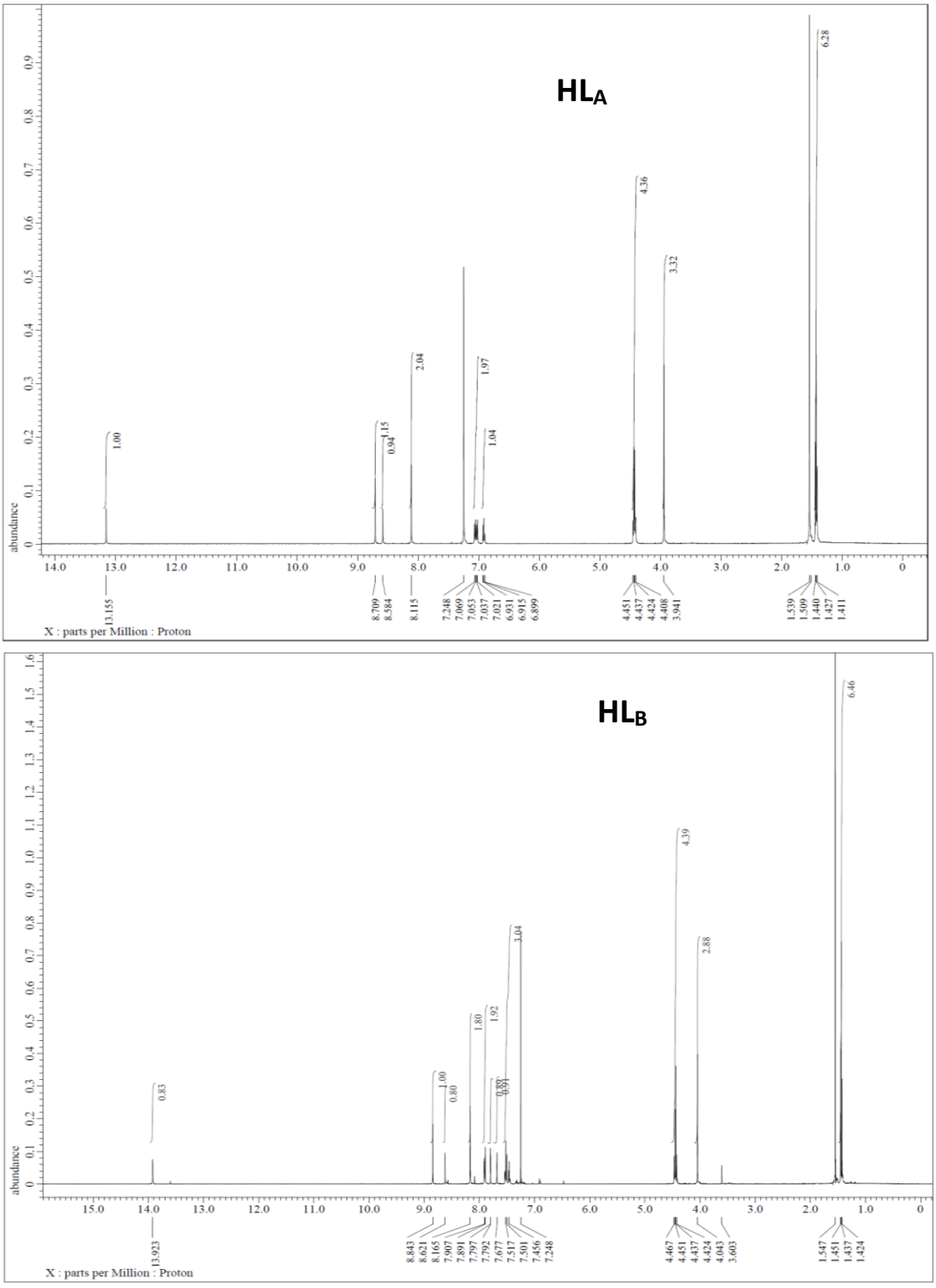

Fig. S3 ^{1}H-NMR spectra (in $CDCl_3$) for (a) **HL$_A$** and (b) **HL$_B$**.

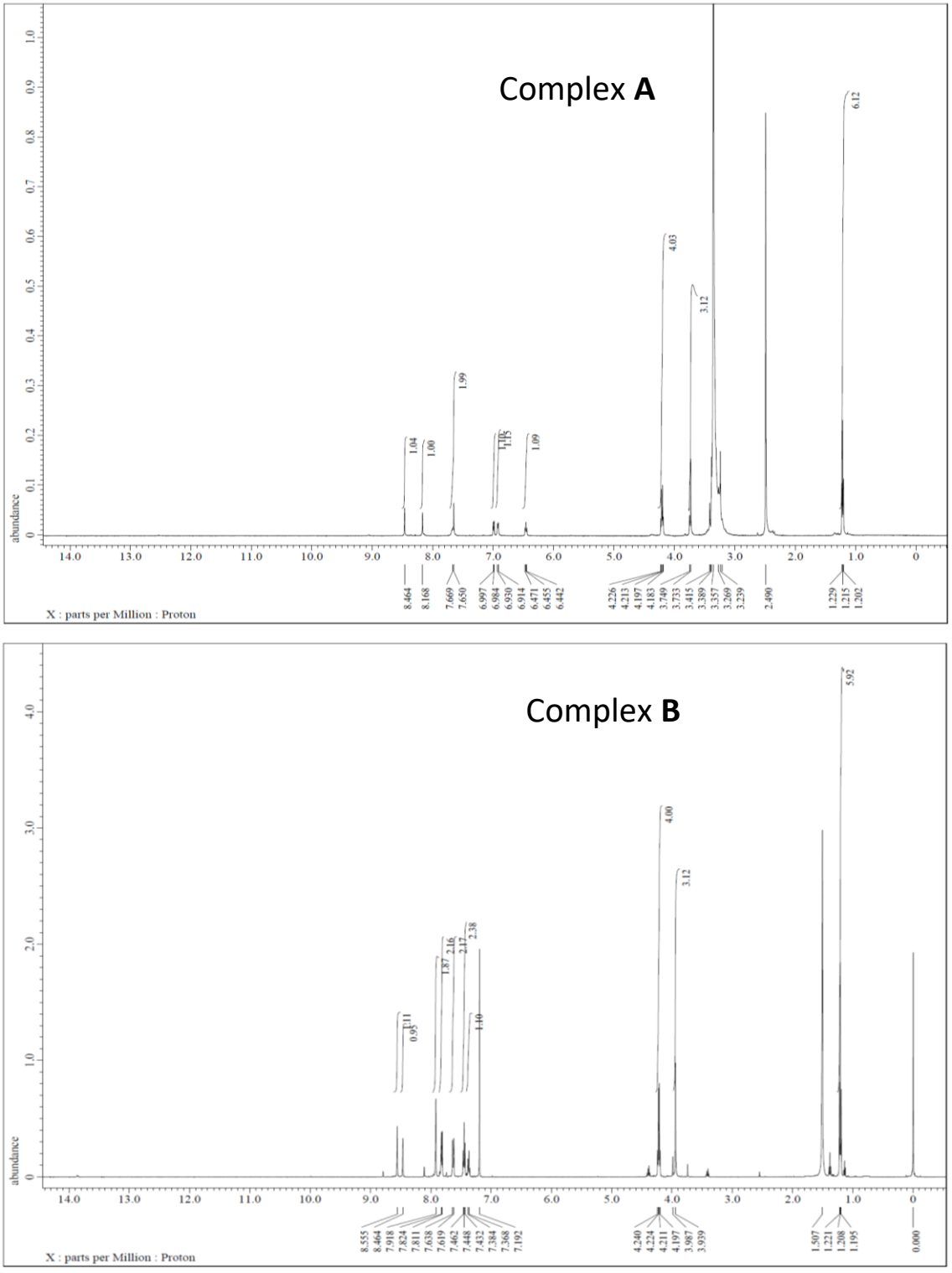

Fig. S4 ^{1}H-NMR spectra (in DMSO-d$_6$) for (a) **A** [$Zn^{II}(L_A)_2$] and (b) **B** [$Zn^{II}(L_B)_2$].

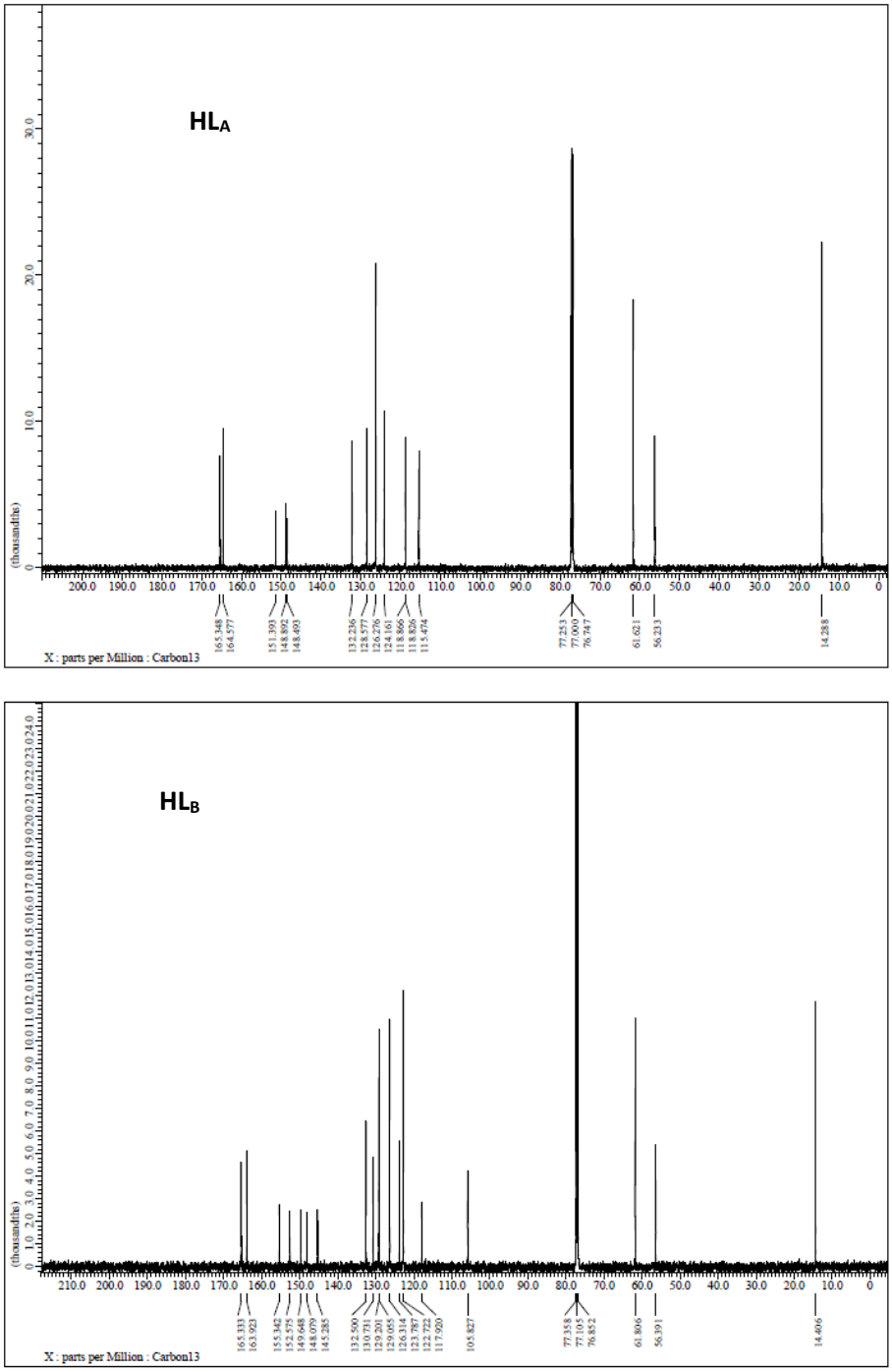

Fig. S5 ^{13}C-NMR spectra for **HL$_A$** and **HL$_B$**.

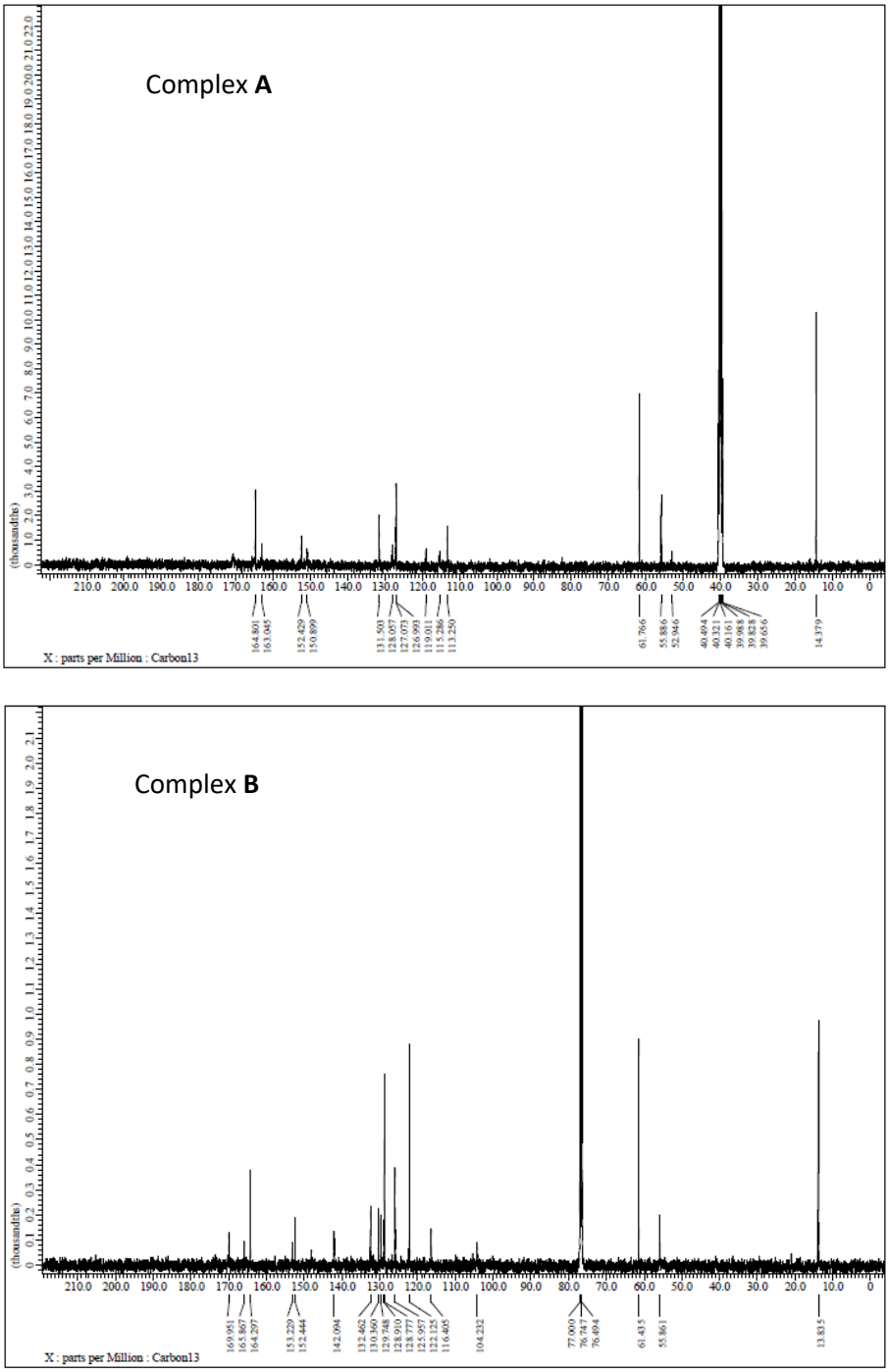

Fig. S6 ^{13}C-NMR spectra for complexes **A** and **B**.

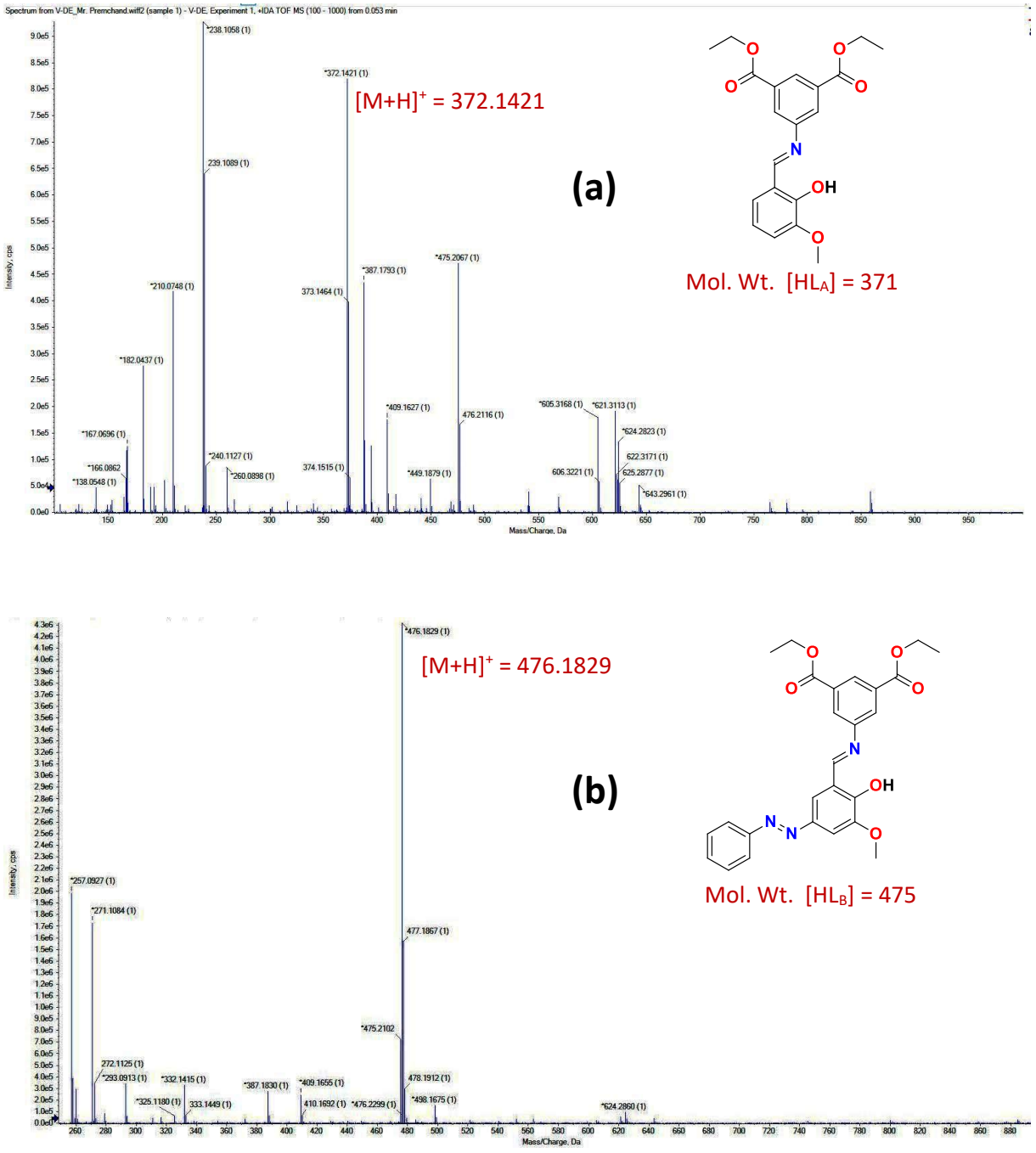

Fig. S7 Mass (HRMS-QTOF) spectra obtained for (a) **HL_A** and (b) **HL_B** in positive mode. Molecular ion peaks were clearly observed with good relative intensity for both which signified the formulation for ligands as $C_{20}H_{21}NO_6$ and $C_{26}H_{25}N_3O_6$, respectively.

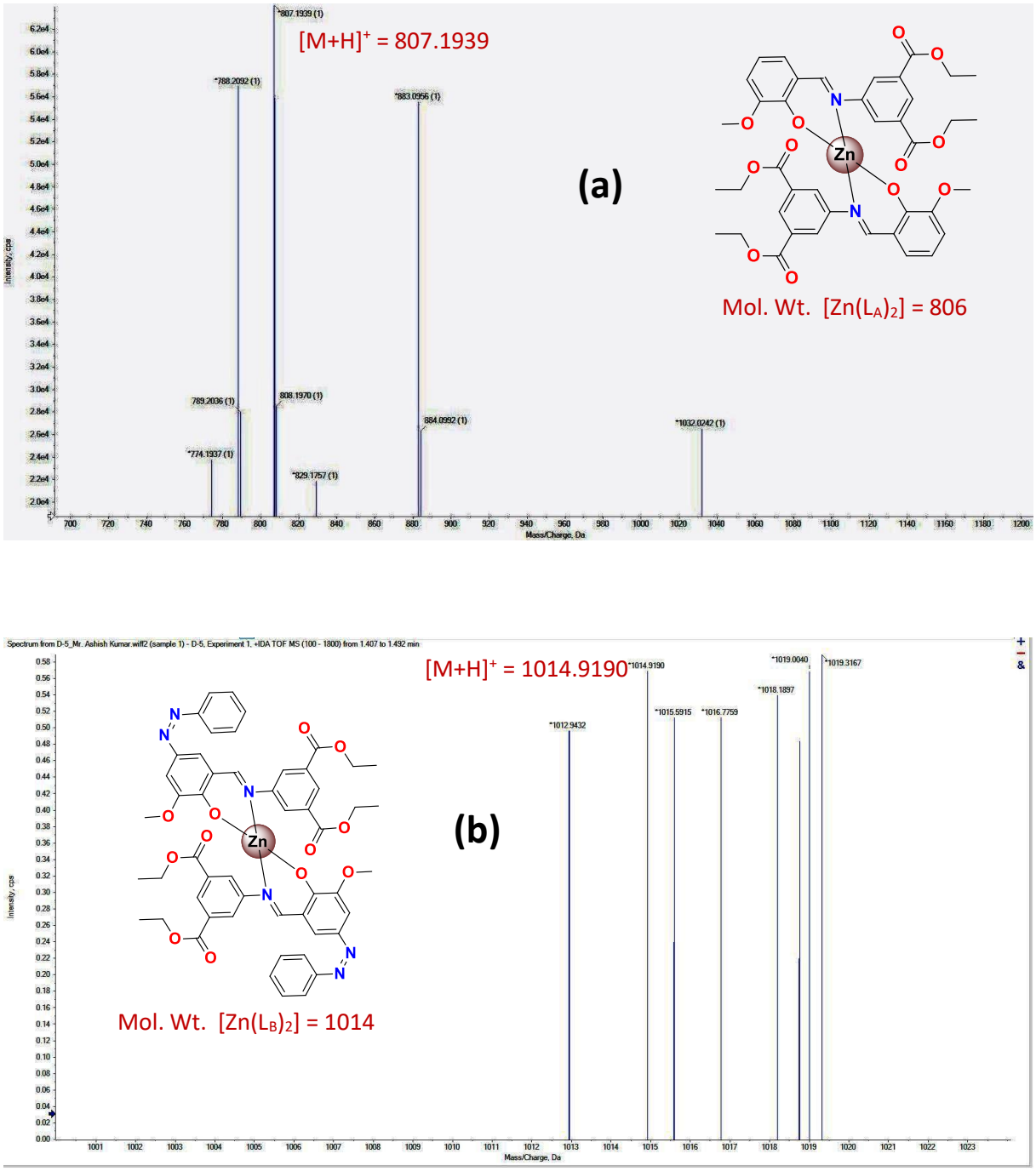

Fig. S8 Mass (HRMS-QTOF) spectra obtained for (a) **A** and (b) **B** in positive mode. Existence of Molecular ion peaks signified their formulations as $C_{40}H_{40}N_2O_{12}Zn$ and $C_{52}H_{48}N_6O_{12}Zn$, respectively.

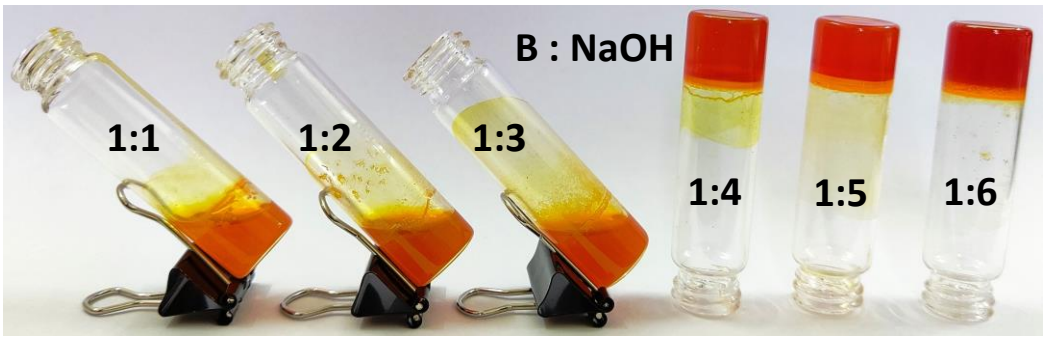

Fig. S9 Gelation for **B** shown in presence of NaOH in different ratios i.e. from 1:1 to 1:6 equiv. and checked via inverted vial method. Appropriate gelation occurred in presence of ≥4.0 equiv. of NaOH.

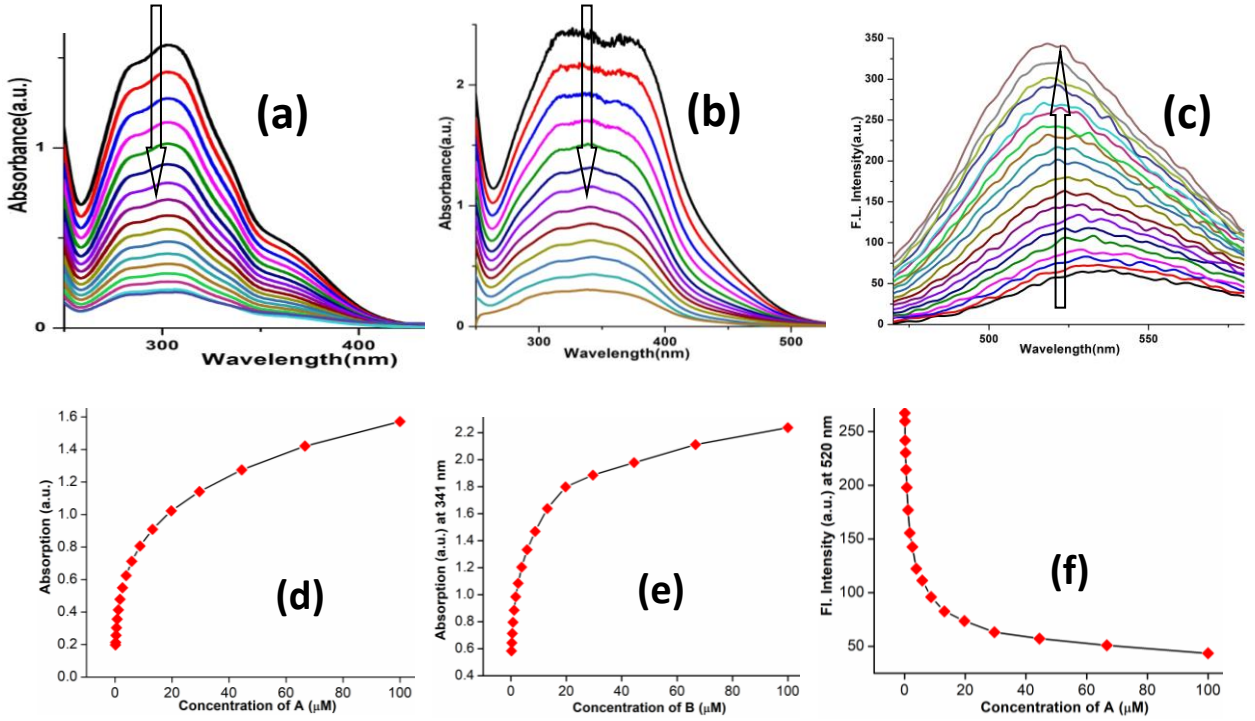

Fig. S10 (a) UV-vis spectra recorded for showing absorbance for **A** and (b) **B** with decrease in concentration from 10^{-4} to ~10^{-7} M called dilution experiments which is one of the basic optimization steps to determine permissible concentration of **A-B** to perform photophysical studies. (c) Similar optimization with dilution of **A** from 10^{-4} to ~10^{-7} M concentration using fluorescence spectroscopy. (d), (e) and (f) display the plots for absorption and emission vs concentration for **A** and **B** at their characteristic wavelengths. (d) Absorbance at 302 nm for **A** (e) Absorbance at 341 nm for **B**. (f) Emission at 520 nm for **A**.

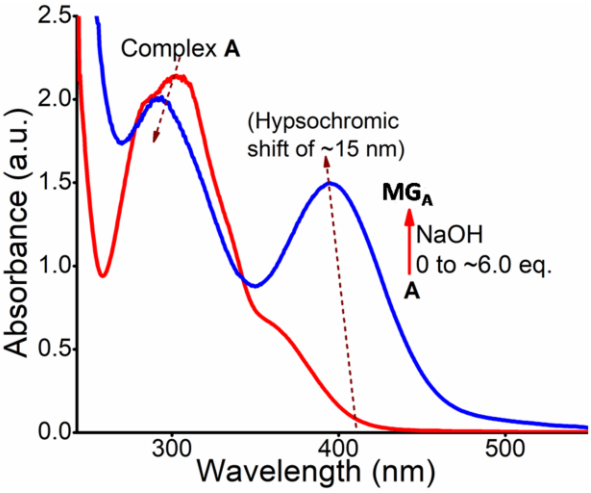

Fig. S11 The first and the last spectra from the UV/vis titration graph for **A** vs NaOH showing significant hypso-chromic shift ($\Delta\lambda$) of ~15 nm on reaching from λ (410 nm) to λ_{gel} (395 nm).

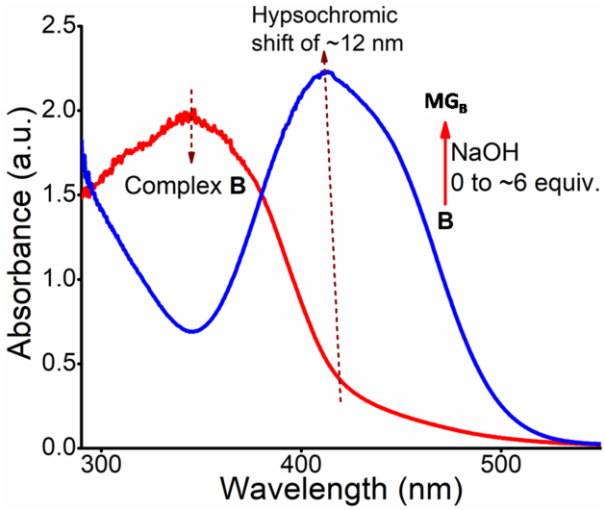

Fig. S12 The first and the last spectra from the UV/vis titration graph for **B** vs NaOH showing significant hypso-chromic shift ($\Delta\lambda$) of 25 nm on reaching from λ (~438 nm) to λ_{gel} (~413 nm).

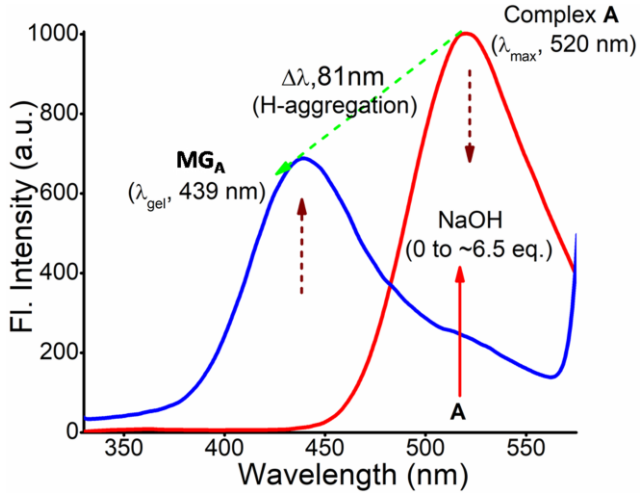

Fig. S13 The first and the last spectra from the fluorescence titration graph for **A** vs NaOH showing significant hypso-chromic shift ($\Delta\lambda$) of ~81 nm on reaching from λ_{max} (520 nm) to λ_{gel} (439 nm).

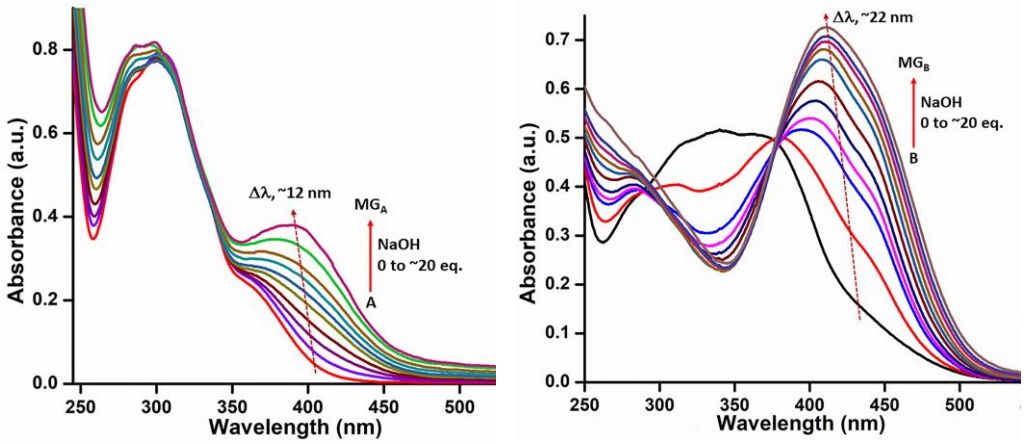

Fig. S14 (a) UV-vis titration for **A** and (b) **B** at ~10^{-7} M concentration in presence of NaOH solution displaying similar hypsochromism with less absorbance.

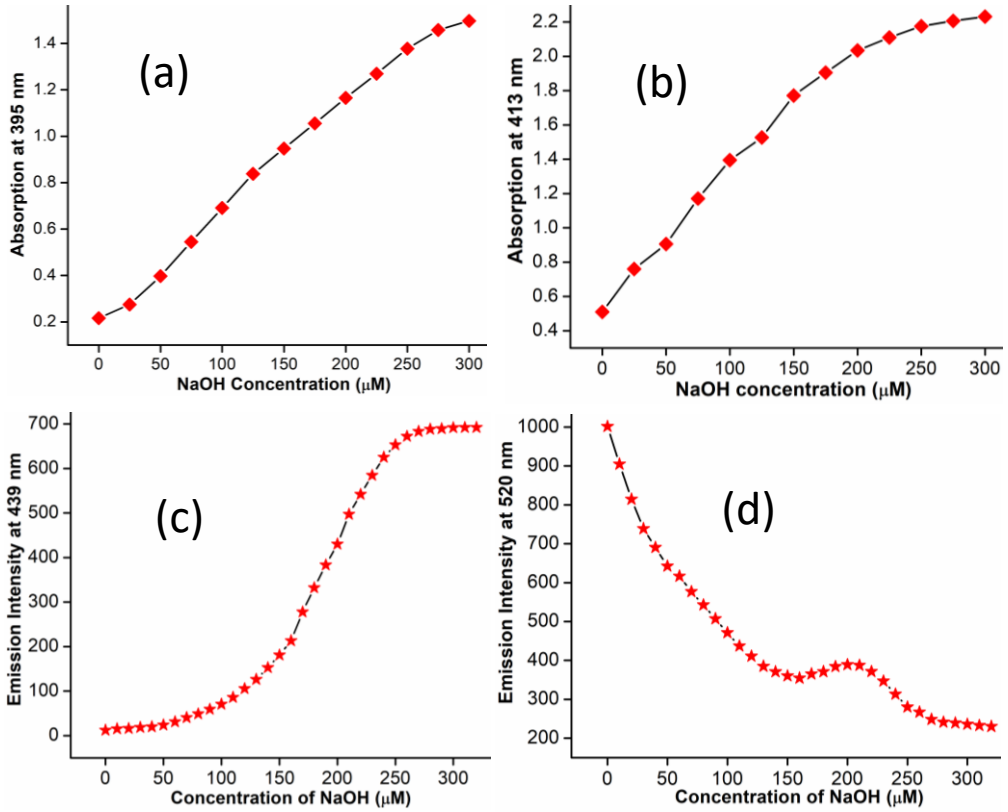

Fig. S15 Additional plots for absorption and emission vs. NaOH concentration at particular wavelength showing (a) Variation of absorption at 395 nm for **A**. (b) Variation of absorption at 413 nm for **B**. (c) Variation of emission at 439 nm for **A** and (d) Variation of emission at 520 nm for **A**.

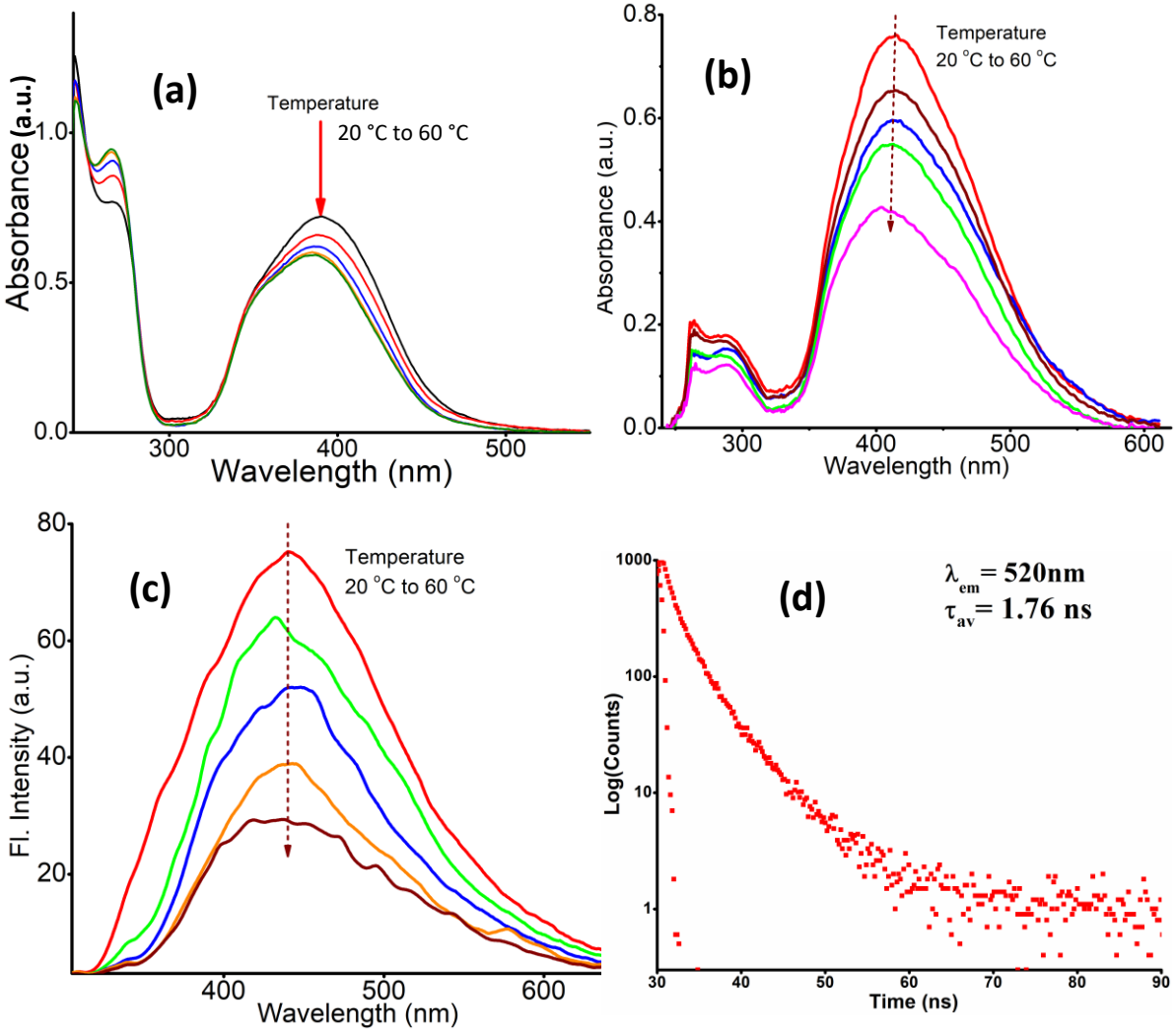

Fig. S16 Temperature dependent UV-vis spectra for (a) **MG$_A$** and (b) **MG$_B$**. (c) Temperature dependent fluorescence spectra for **MG$_A$**. (d) Fluorescence decay graph for complex **A**.

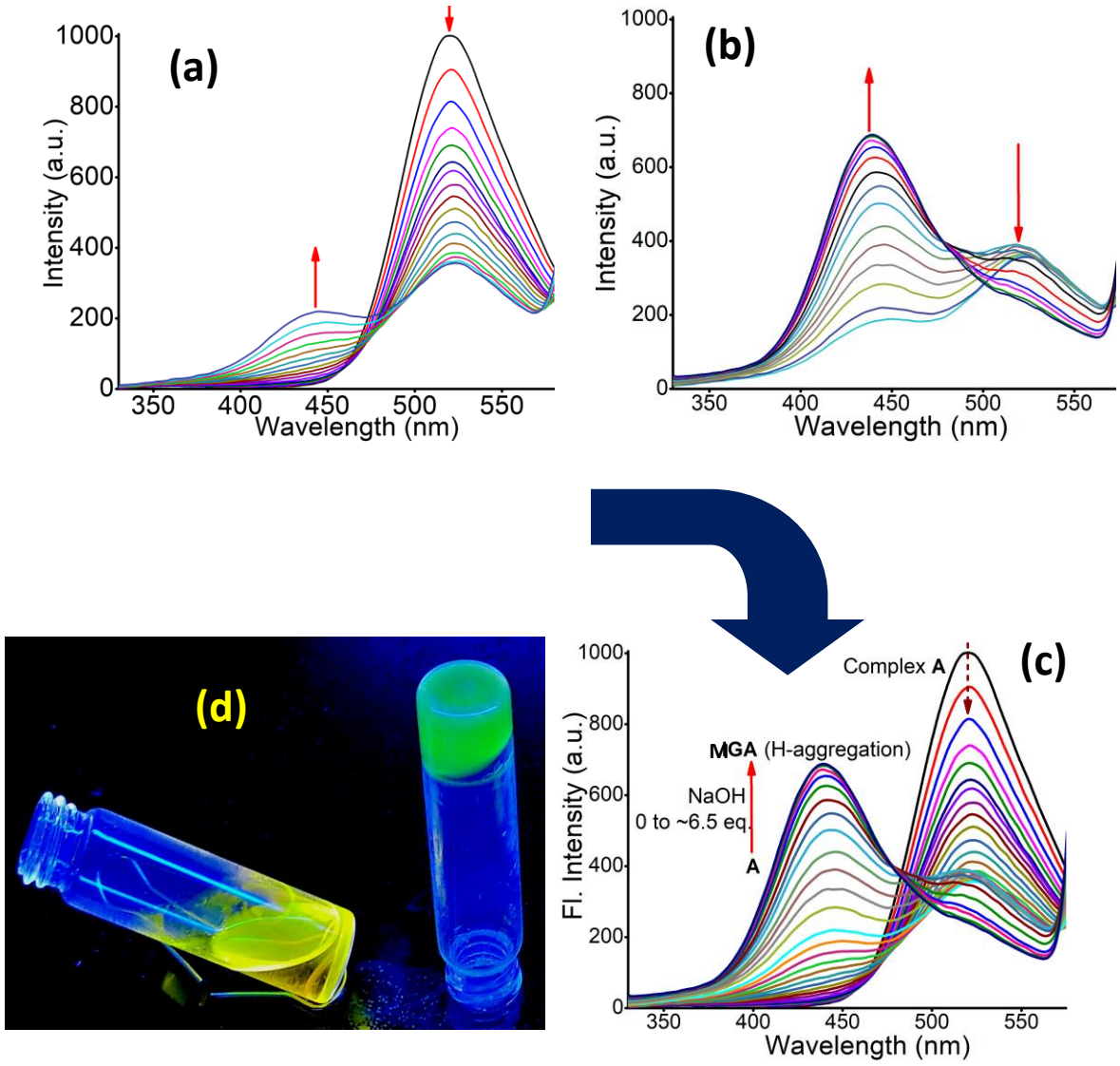

Fig. S17 (a) First half of fluorescence titration for **A**+NaOH displaying conversion of esters into carboxylates. (b) Second half of fluorescence titration spectra for **A**+NaOH signifying the CT followed by aggregation. It substantiated that aggregation started to occur after a threshold conversion of **A** into $\mathbf{MG_A}$ via conformational transformation called as AICT (c) Combined full titration spectra showing the gelation of **A**.

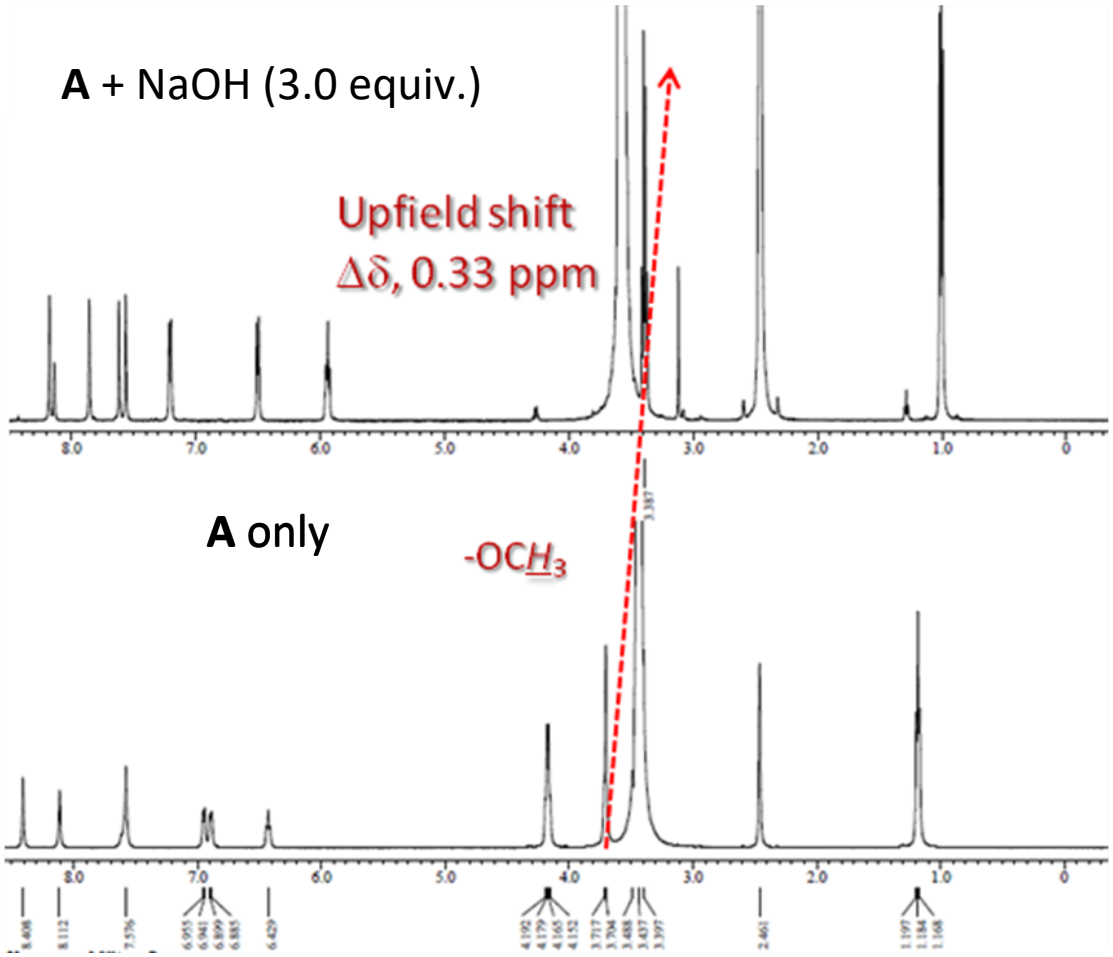

Fig. S18 A portion from ^{1}H NMR titration spectra for **A** in presence of 3.0 equiv. of NaOH showing significant upfield shift of signal associated with –OCH_3 proton ($\Delta\delta$, 0.33 ppm). It is indicative of a significant conformational transformation induced in presence of NaOH as a result of ester to carboxylate conversion.

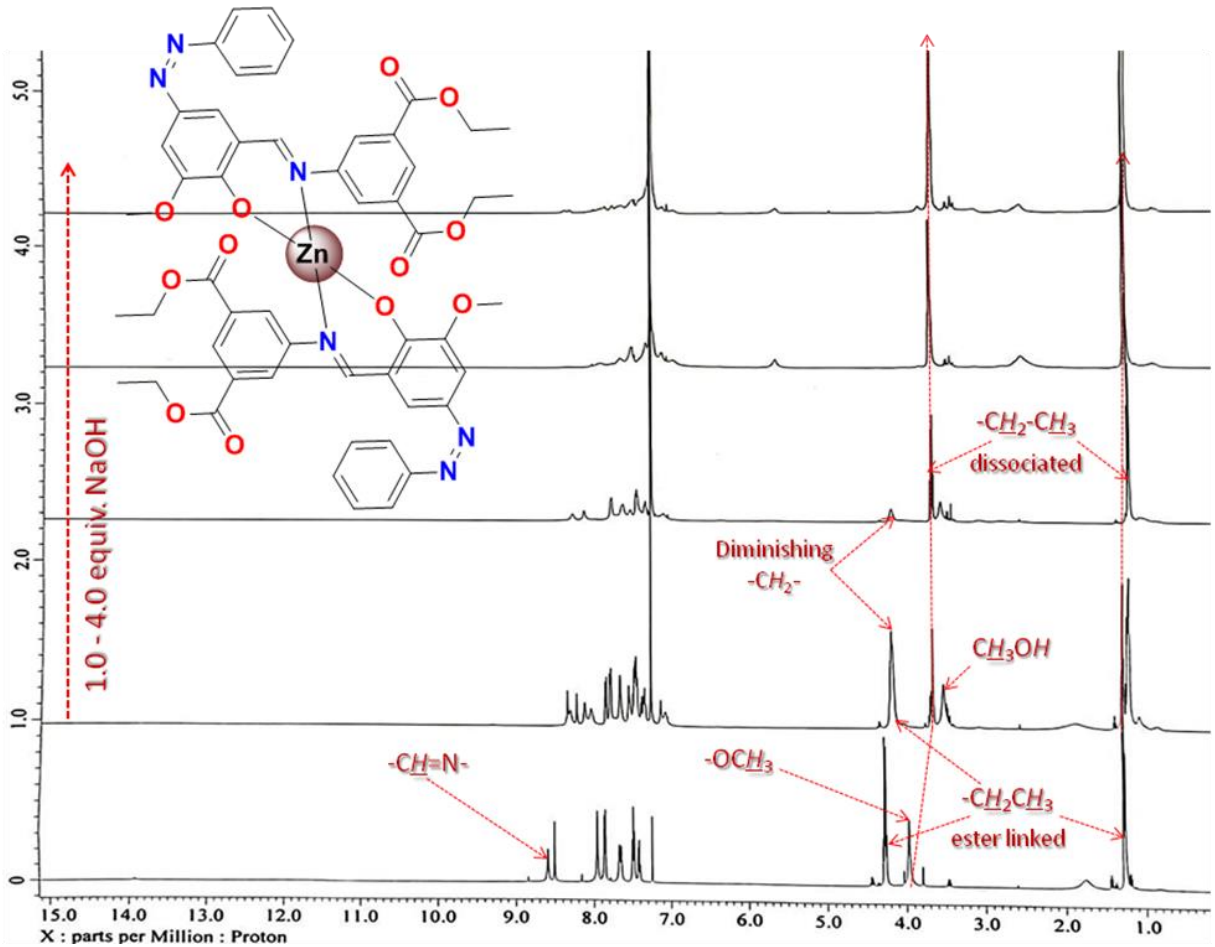

Fig. S19 ^{1}H NMR titration spectra for **B** ($CDCl_3$) + NaOH (CD_3OD; 0 - 4.0 equiv.). Similar changes were evident as observed for **A** + NaOH except that the signal for -C*H*=N- (δ, 8.59 ppm) did not disappear (possibly due to $CDCl_3$ bond did not break) but undergone upfield shifting and broadening those might be relevant for planar π-interactions.

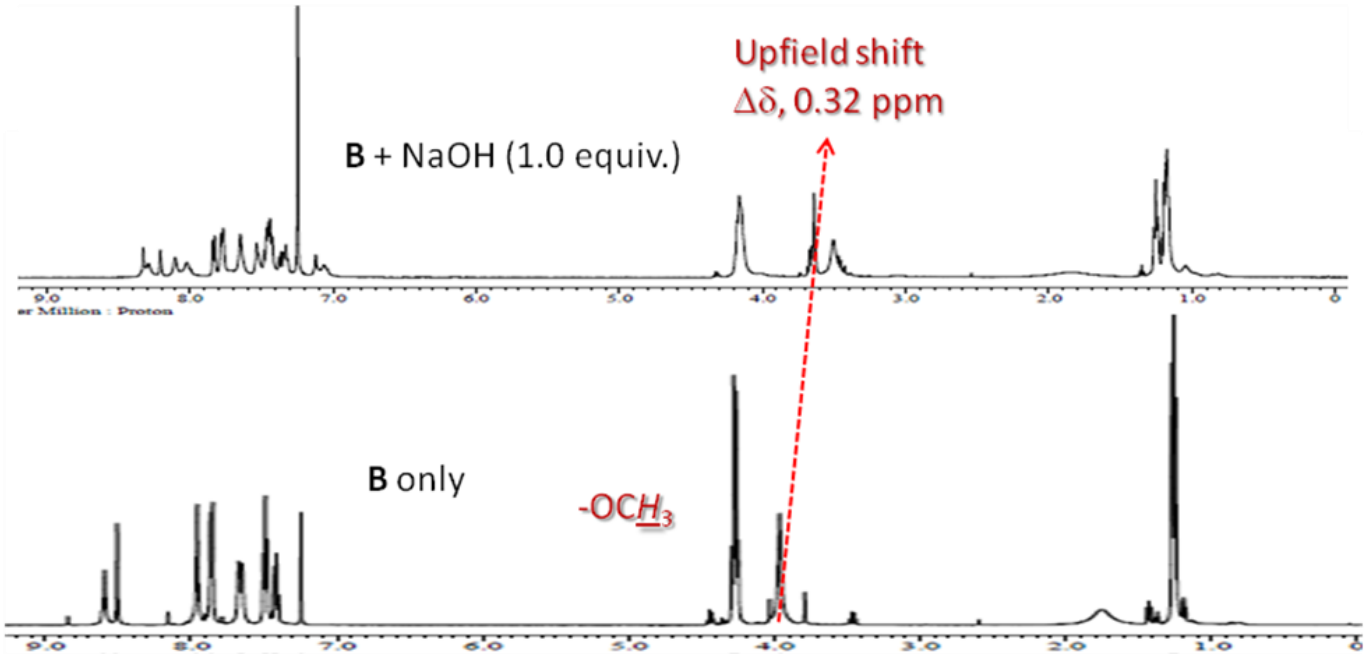

Fig. S20 A portion from ^{1}H NMR titration spectra for **B** in presence of 1.0 equiv. of NaOH showing significant upfield shift of signal associated with –OCH_3 proton ($\Delta\delta$, 0.32 ppm). It substantiated a significant tendency towards conformational transformations induced by NaOH as indicated for **A** + NaOH.

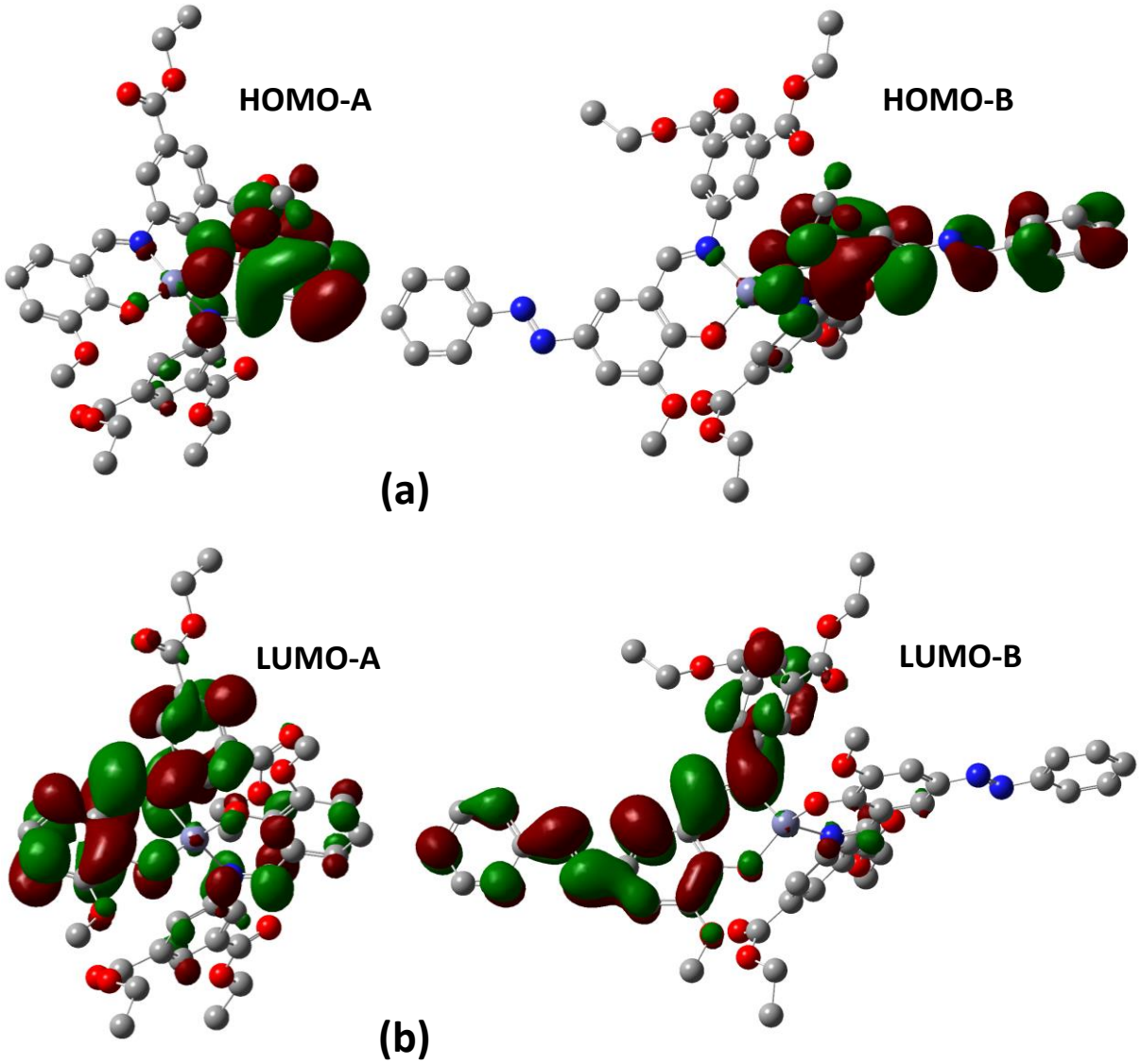

Fig. S21 DFT optimized structures representing (a) HOMO of **A** (Left hand side) and **B** (Right hand side) and (b) LUMO of **A** (Left hand side) and **B** (Right hand side). The theoretically optimized structures exhibited t_d coordination geometry around Zn^{II}. It was observed that most of the electron density is localized mainly on the o-vanillin core (in **A**) and p-a-p (in **B**) suggesting that the electron density has preferred to stabilize away from metal centre which induced a charge separation and thereby dipole moment. It was considered as a key factor for induced gelation under saponification conditions.

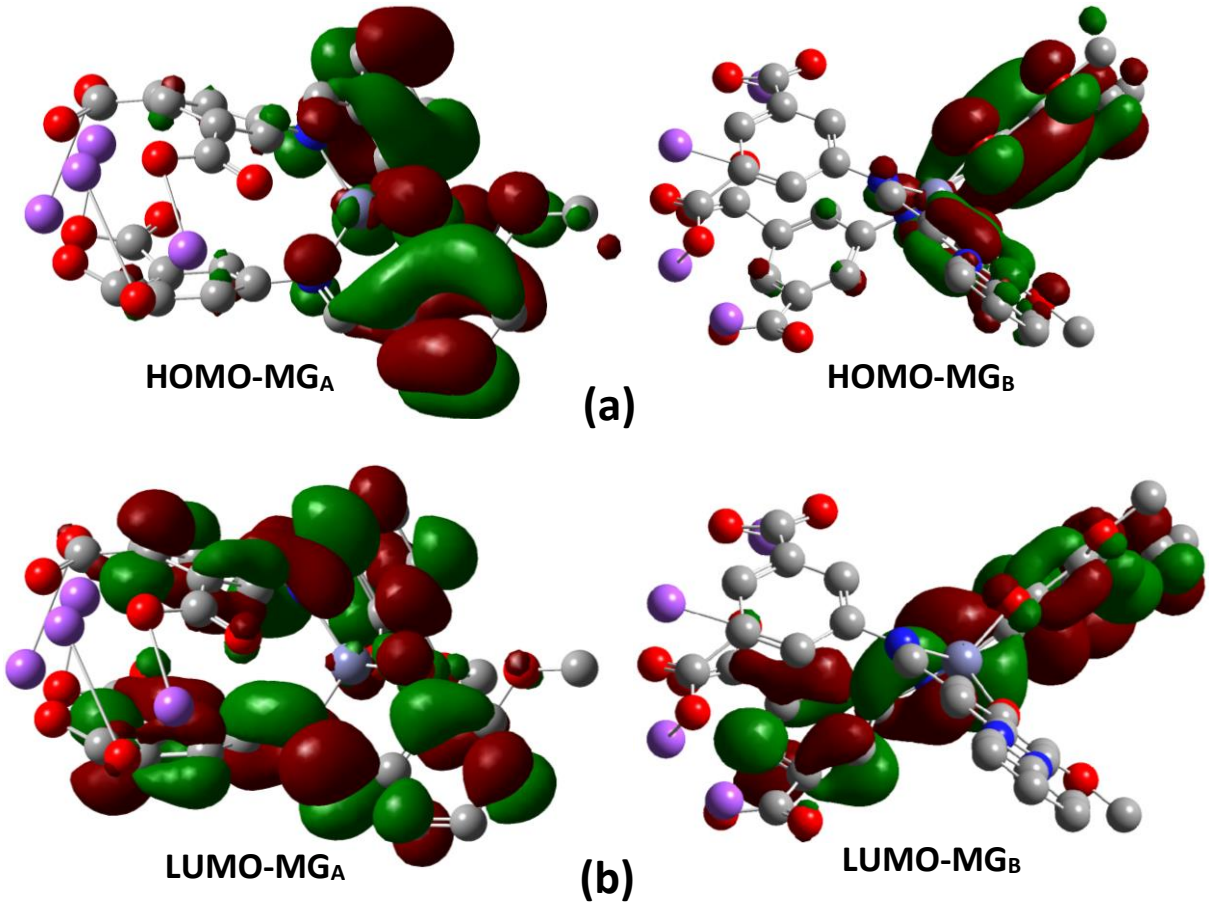

Fig. S22 DFT optimized structures representing the progelators (a) HOMO of **MG$_A$** (Left hand side) and **MG$_B$** (Right hand side) and (b) LUMO of **MG$_A$** (Left hand side) and **MG$_B$** (Right hand side). These displayed similar t_d geometrical environment around the metal centre but entirely different from their parent complexes **A** and **B** in their conformational arrangements. Most of the *e*-den is localized on the o-vanillin core (**A**) and pap core (**B**) suggesting that *e*-den is stabilized away from the metal centre which consequently caused charge separation between the centre and the periphery. It has been considered as a key factor for gelation to take place under saponification induced conditions.

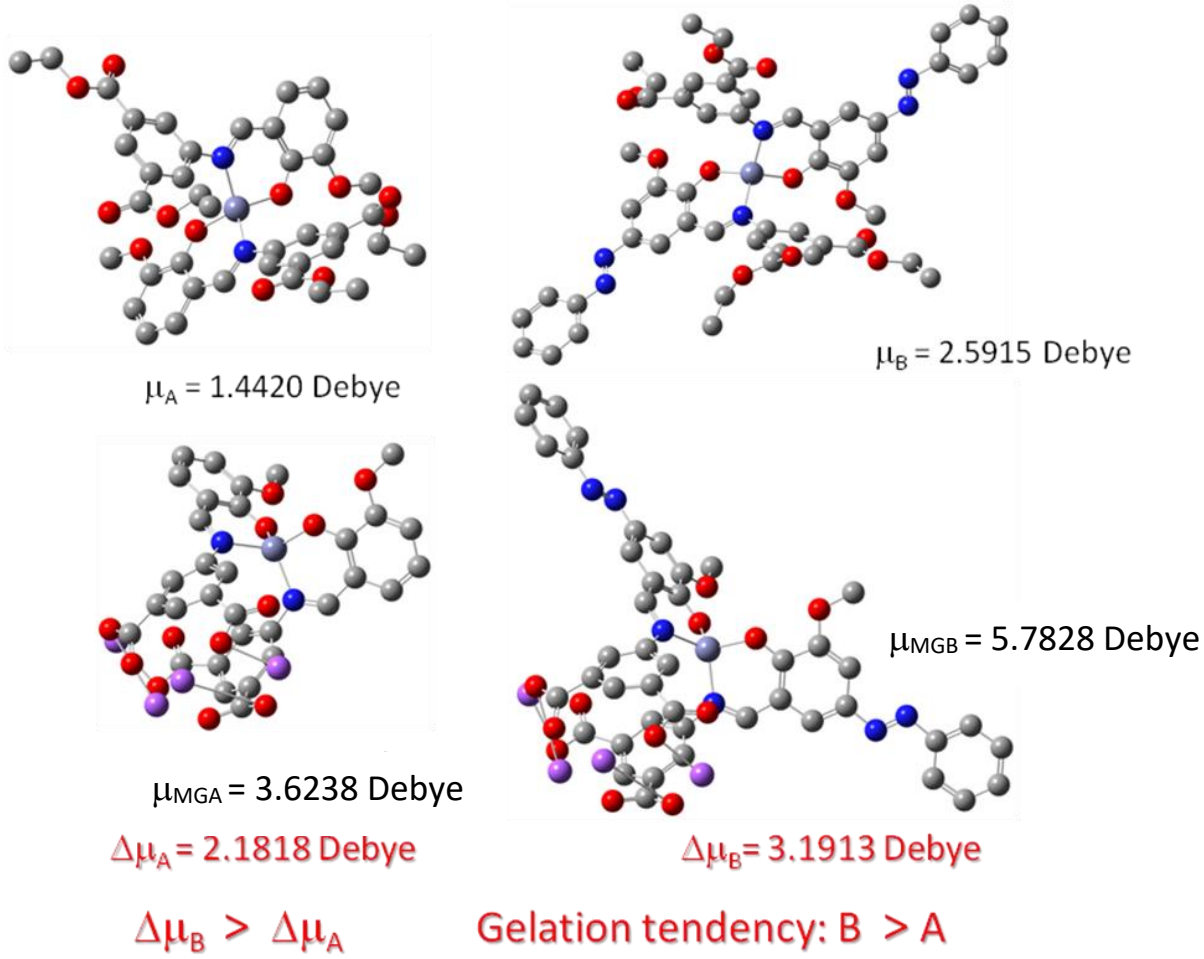

Fig. S23 DFT optimized structures of **A**-**B** and **MG$_A$**-**MG$_B$** (hydrogens are omitted for clarity). Theoretical studies revealed that each couple of the complex (**A** and **B**) and corresponding saponified products (**MG$_A$**-**MG$_B$**) exhibits differences in dipole moments i.e. 2.18 and 3.19 Debye for **A-MG$_A$** and **B-MG$_B$** pairs, respectively. Therefore, it substantiated their comparative tendencies towards gelation as **B** > **A** which explained the fact why complex **A** took more time to undergo gelation as compared to **B**. This fact has also been reasoned by observing large (4.082 Å) and small (4.073 Å) centroid-centroid distances in **MG$_A$** and **MG$_B$**, respectively substantiating increasing gelation efficiency from **A** to **B**.

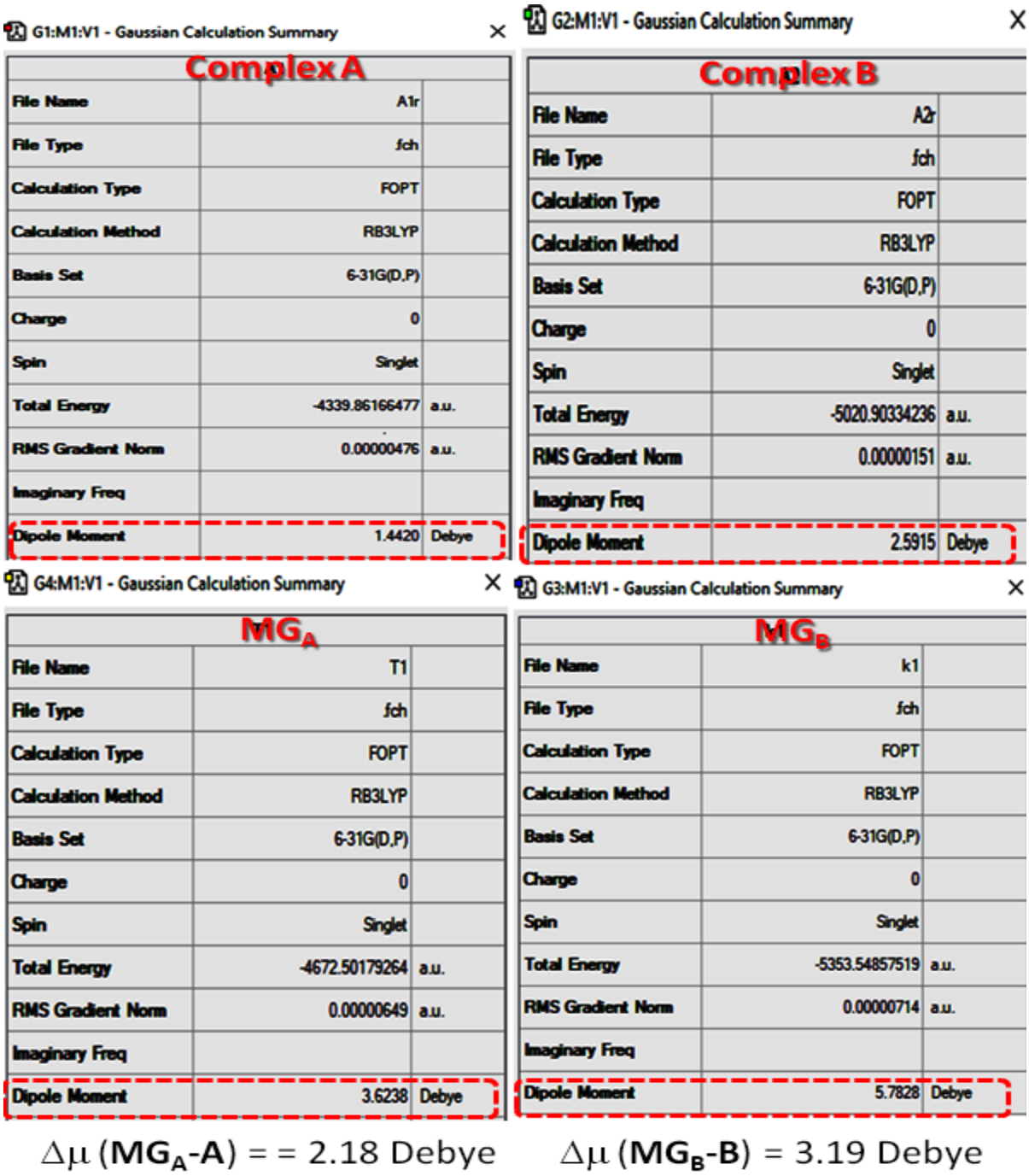

Fig. S24 Result summaries obtained from DFT optimization for model structures of **A-B** and **MG$_A$-MG$_B$** showing their dipole moments. A substantial increase in dipole moment observed in the order Δμ (**MG$_B$–B**) > Δμ (**MG$_A$–A**) indicated gelation efficiency for **B** > **A**.

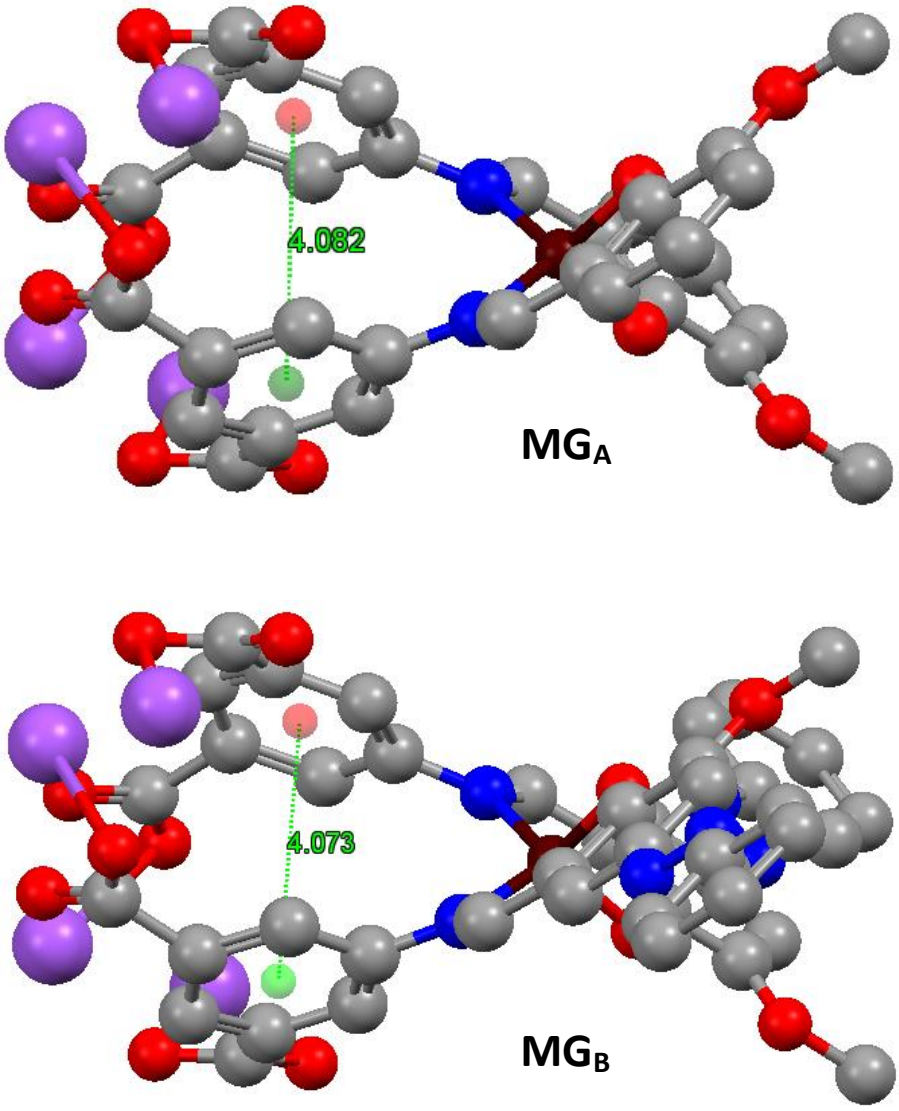

Fig. S25 DFT optimized structures of **MG$_A$-MG$_B$** (hydrogens are omitted for clarity) to show the difference in centroid-centroid distances between the respective isophthalate rings.

Table T1. Crystal data and structure refinement for **HL_B**.

Identification code	shelxl	
Empirical formula	$C_{26}\ H_{25}\ N_3O_6$	
Formula weight	951.010	
Temperature	293(2) K	
Wavelength	0.71073 Å	
Crystal system	Triclinic	
Space group	*P* -1	
Unit cell dimensions	a = 7.52118 (14) Å	α= 62.200 (2)°
	b = 19.1168 (4) Å	β= 80.9796 (15)°
	c = 19.7439 (4) Å	γ = 87.5397 (16)°
Volume	2478.6 (1) $Å^3$	
Z	2	
Density (calculated)	1.274 g/cm^3	
Absorption coefficient (μ)	0.092 mm^{-1}	
F(000)	1000	
Crystal size	0.20 x 0.10 x 0.05 mm^3	
Theta range for data collection	2.04 to 25.00°.	
Reflections collected	71966	
Independent reflections	8723 [R(int) = 0.0311]	
Data completeness	1.000	
Absorption correction	Semi-empirical from equivalents	
Max. and min. transmission	0.989 and 0.995	
Refinement method	Full-matrix least-squares on F^2	
Data / restraints / parameters	8723 / 357 / 796	
Goodness-of-fit on F^2	1.0566	
Final R indices [I>2σ(I)]	R1 = 0.0619, wR2 = 0.1920	
R indices (all data)	R1 = 0.0948, wR2 = 0.2175	
Largest peak and deepest hole	0.7678 and -0.2667 $e.Å^{-3}$	

Table T2. Selected bond lengths [Å] and bond angles [º] for **HL_B**.

Atom	Atom	Length/Å	Atom	Atom	Length/Å	Atom	Atom	Length/Å
C1	C2	1.383(3)	C15	C16	1.414(3)	N2	C18	1.434(3)
C1	C6	1.386(3)	C16	C17	1.368(3)	N3	C21	1.439(3)
C2	C3	1.383(3)	C17	C18	1.396(3)	O1	C7	1.326(3)
C2	C7	1.489(3)	C18	C19	1.371(3)	O1	C8	1.460(3)
C3	C4	1.387(3)	C21	C22	1.383(4)	O2	C7	1.206(3)
C4	C5	1.391(3)	C21	C26	1.369(3)	O3	C10	1.323(3)
C5	C6	1.387(3)	C22	C23	1.385(4)	O3	C11	1.458(3)
C6	C10	1.490(3)	C23	C24	1.367(4)	O4	C10	1.190(3)
C8	C9	1.475(4)	C24	C25	1.368(4)	O5	C16	1.363(3)
C11	C12	1.405(5)	C25	C26	1.369(4)	O5	C20	1.423(3)
C13	C14	1.440(3)	N1	C4	1.419(3)	O6	C15	1.334(3)
C14	C15	1.401(3)	N1	C13	1.273(3)			
C14	C19	1.391(3)	N2	N3	1.241(3)			

Atom	Atom	Atom	Angle/°	Atom	Atom	Atom	Angle/°
C1	C6	C10	118.4(2)	C22	C21	C26	120.1(2)
C1	C2	C3	119.6(2)	C23	C24	C25	119.3(3)
C1	C6	C5	120.4(2)	C24	C25	C26	120.7(3)
C1	C2	C7	122.8(2)	N1	C13	C14	122.4(2)
C2	C3	C4	121.2(2)	N1	C4	C3	116.3(2)
C2	C1	C6	119.8(2)	N1	C4	C5	124.8(2)
C3	C4	C5	118.9(2)	N2	C18	C17	125.0(2)
C3	C2	C7	117.6(2)	N2	C18	C19	115.0(2)
C4	N1	C13	123.2(2)	N2	N3	C21	112.8(2)
C4	C5	C6	120.0(2)	N3	N2	C18	114.2(2)
C5	C6	C10	121.2(2)	N3	C21	C22	123.8(2)
C7	O1	C8	116.07(19)	N3	C21	C26	116.1(2)
C10	O3	C11	117.3(2)	O1	C7	C2	113.5(2)
C13	C14	C15	121.0(2)	O1	C8	C9	108.4(2)
C13	C14	C19	120.1(2)	O1	C7	O2	123.0(2)
C14	C15	C16	119.6(2)	O2	C7	C2	123.5(2)
C14	C19	C18	121.2(2)	O3	C11	C12	109.3(3)
C15	C16	C17	120.0(2)	O3	C10	C6	112.2(2)
C15	C14	C19	118.9(2)	O3	C10	O4	123.6(2)
C16	C17	C18	120.2(2)	O4	C10	C6	124.1(2)
C16	O5	C20	118.2(2)	O5	C16	C15	114.1(2)
C17	C18	C19	120.0(2)	O5	C16	C17	125.8(2)
C21	C22	C23	118.6(3)	O6	C15	C14	122.2(2)
C21	C26	C25	120.2(3)	O6	C15	C16	118.3(2)
C22	C23	C24	121.1(3)				

Table T3. Crystal data and structure refinement for Complex **B**.

Identification code	shelxl	
Empirical formula	$C_{52}\ H_{48}\ N_6\ O_{12}\ Zn$	
Formula weight	1012.26	
Temperature	293 (2) K	
Wavelength	0.71073 Å	
Crystal system	Triclinic	
Space group	*P* -1	
Unit cell dimensions	a = 15.0993 (2) Å	α = 100.281 (2)°
	b = 17.6129 (4) Å	β = 90.399 (2)°
	c = 20.3424 (5) Å	γ = 102.672 (2)°
Volume	5187.4 (2) $Å^3$	
Z	4	
Density (calculated)	1.299 g/cm^3	
Absorption coefficient	0.539 mm^{-1}	
F(000)	2112	
Crystal size	0.30 x 0.15 x 0.08 mm^3	
Theta range for data collection	2.397 to 23.000°.	
Reflections collected	120591	
Independent reflections	14424 [R(int) = 0.0582]	
Data completeness	0.998	
Absorption correction	Semi-empirical from equivalents	
Refinement method	Full-matrix least-squares on F^2	
Data / restraints / parameters	14424 / 455 / 1444	
Goodness-of-fit on F^2	1.0150	
Final R indices [I>2sigma(I)]	R1 = 0.0607	
R indices (all data)	R1 = 0.0995, wR2 = 0.1935	
Largest diff. peak and hole	0.7100 and -0.4200 e.$Å^{-3}$	

Table T4. Selected bond lengths [Å] and bond angles [º] for Complex **B**.

Atom	Atom	Length/Å	Atom	Atom	Length/Å	Atom	Atom	Length/Å	Atom	Atom	Length/Å
C1	C2	1.400(6)	C15	O5	1.294(5)	C32	C27	1.389(6)	C44	N5	1.427(6)
C1	C6	1.382(6)	C16	C15	1.433(6)	C32	C31	1.378(7)	C46	O12	1.434(6)
C1	N1	1.418(5)	C16	O6	1.359(5)	C33	O7	1.186(7)	C47	C52	1.362(8)
C3	C2	1.378(6)	C17	C16	1.370(6)	C33	O8	1.325(8)	C47	N6	1.462(7)
C3	C4	1.373(6)	C17	C18	1.403(7)	C34	O8	1.471(9)	C48	C47	1.360(8)
C3	C7	1.497(7)	C18	N2	1.421(6)	C35	C34	1.140(14)	C48	C49	1.376(9)
C4	C5	1.390(6)	C19	C14	1.426(6)	C36	C31	1.493(8)	C50	C49	1.340(10)
C5	C6	1.384(6)	C19	C18	1.354(7)	C36	O10	1.311(7)	C50	C51	1.366(10)
C7	O1	1.206(6)	C20	O6	1.423(6)	C36	O9	1.215(7)	C51	C52	1.374(8)
C7	O2	1.312(6)	C22	C21	1.324(10)	C37	C38	1.454(9)	O11	Zn1	1.917(3)
C8	O2	1.457(6)	C23	C22	1.415(10)	C37	O10	1.458(7)	O5	Zn1	1.912(3)
C9	C8	1.437(10)	C24	C23	1.284(14)	C39	C40	1.425(6)	N1	Zn1	2.009(3)
C10	C5	1.486(7)	C25	C24	1.353(14)	C40	C45	1.419(6)	N3	C21	1.442(7)
C10	O3	1.205(6)	C25	C26	1.419(12)	C41	C40	1.399(6)	N3	N2	1.250(6)
C10	O4	1.306(6)	C26	C21	1.370(10)	C41	O11	1.302(5)	N4	C27	1.439(6)
C11	O4	1.456(7)	C28	C27	1.383(6)	C42	C41	1.429(6)	N4	C39	1.303(5)
C12	C11	1.418(10)	C29	C28	1.379(7)	C42	C43	1.382(6)	N4	Zn1	2.012(4)
C13	N1	1.303(5)	C29	C30	1.374(7)	C42	O12	1.360(6)	N6	N5	1.231(6)
C14	C13	1.419(6)	C29	C33	1.484(8)	C44	C43	1.393(7)			
C14	C15	1.418(6)	C30	C31	1.380(7)	C44	C45	1.346(7)			

Atom	Atom	Atom	Angle/°	Atom	Atom	Atom	Angle/°	Atom	Atom	Atom	Angle/°
C1	N1	Zn1	119.1(3)	C14	C15	C16	118.0(4)	C28	C27	C32	119.1(4)
C1	C6	C5	120.5(4)	C15	O5	Zn1	126.8(3)	C28	C27	N4	116.7(4)
C2	C1	N1	124.0(4)	C15	C14	C13	124.3(4)	C28	C29	C33	122.8(6)
C2	C3	C7	120.6(5)	C15	C14	C19	118.7(4)	C29	C28	C27	120.7(5)
C3	C4	C5	119.7(4)	C16	O6	C20	117.5(4)	C29	C30	C31	120.6(5)
C3	C2	C1	119.9(4)	C16	C17	C18	119.9(4)	C30	C31	C36	118.4(5)
C4	C5	C10	119.7(5)	C17	C16	C15	121.3(4)	C30	C29	C28	119.6(5)
C4	C3	C2	120.7(4)	C17	C18	N2	123.7(5)	C30	C29	C33	117.6(6)
C4	C3	C7	118.6(5)	C18	C19	C14	121.4(4)	C31	C32	C27	120.4(5)
C6	C5	C4	119.9(4)	C19	C18	C17	120.6(4)	C32	C27	N4	124.2(4)
C6	C5	C10	120.5(5)	C19	C18	N2	115.7(5)	C32	C31	C30	119.7(5)
C6	C1	C2	119.2(4)	C21	C22	C23	119.6(9)	C32	C31	C36	121.9(5)
C6	C1	N1	116.8(4)	C21	C26	C25	119.5(10)	C33	O8	C34	114.9(7)
C7	O2	C8	116.8(5)	C22	C21	C26	120.0(7)	C35	C34	O8	115.1(13)
C9	C8	O2	108.1(6)	C22	C21	N3	124.5(7)	C36	O10	C37	115.9(5)
C10	O4	C11	117.2(5)	C23	C24	C25	122.5(11)	C38	C37	O10	107.8(6)
C12	C11	O4	107.0(6)	C24	C23	C22	120.6(11)	C39	N4	C27	119.3(4)
C13	N1	C1	119.7(4)	C24	C25	C26	117.7(10)	C39	N4	Zn1	117.9(3)
C13	N1	Zn1	121.1(3)	C26	C21	N3	115.5(7)	C40	C41	C42	117.8(4)

Atom	Atom	Atom	Angle/°	Atom	Atom	Atom	Angle/°	Atom	Atom	Atom	Angle/°
C13	C14	C19	117.0(4)	C27	N4	Zn1	122.7(3)	C41	O11	Zn1	123.8(3)
C41	C40	C45	118.8(4)	C52	C47	N6	124.8(6)	O5	C15	C14	124.6(4)
C41	C40	C39	125.6(4)	N1	Zn1	N4	118.13(15)	O5	C15	C16	117.4(4)
C42	O12	C46	117.4(4)	N1	C13	C14	127.8(4)	O6	C16	C17	125.9(4)
C42	C43	C44	119.6(5)	N2	N3	C21	112.4(5)	O6	C16	C15	112.8(4)
C43	C42	C41	121.4(5)	N3	N2	C18	114.0(5)	O7	C33	O8	123.2(7)
C43	C44	N5	125.8(5)	N4	C39	C40	128.8(4)	O7	C33	C29	125.2(8)
C44	C45	C40	122.3(5)	N5	N6	C47	112.4(5)	O8	C33	C29	111.6(6)
C45	C40	C39	115.6(4)	N6	N5	C44	113.9(5)	O9	C36	O10	124.2(6)
C45	C44	C43	120.0(4)	O1	C7	O2	124.8(5)	O9	C36	C31	122.3(6)
C45	C44	N5	114.2(5)	O1	C7	C3	122.1(5)	O10	C36	C31	113.5(6)
C47	C52	C51	118.9(7)	O2	C7	C3	113.1(5)	O11	Zn1	N1	117.38(14)
C47	C48	C49	120.2(7)	O3	C10	O4	123.5(5)	O11	Zn1	N4	97.22(14)
C48	C47	C52	120.3(6)	O3	C10	C5	124.1(5)	O11	C41	C40	124.5(4)
C48	C47	N6	114.9(6)	O4	C10	C5	112.4(5)	O11	C41	C42	117.7(4)
C49	C50	C51	120.3(7)	O5	Zn1	O11	115.09(14)	O12	C42	C43	124.5(5)
C50	C49	C48	119.7(7)	O5	Zn1	N1	94.85(13)	O12	C42	C41	114.1(4)
C50	C51	C52	120.5(7)	O5	Zn1	N4	115.63(14)				